HIGHLIGHT

Does Conventional Nucleation Occur during Phase Separation in Polymer Blends?

NITASH P. BALSARA,[1–3] TIMOTHY J. RAPPL,[1] AMY A. LEFEBVRE[1]

[1]Department of Chemical Engineering, University of California, Berkeley, California 94720

[2]Material Sciences Division, Lawrence Berkeley National Laboratory, University of California, Berkeley, California 94720

[3]Environmental Energies Technologies Division, Lawrence Berkeley National Laboratory, University of California, Berkeley, California 94720

Received 22 September 2003; revised 15 December 2003; accepted 15 December 2003
DOI: 10.1002/polb.20055
Published online in Wiley InterScience (www.interscience.wiley.com).

ABSTRACT: The kinetics of liquid–liquid phase separation in off-critical polymer blends was studied with time-resolved small-angle neutron scattering. Our objective was to study the nature of the nuclei that formed during the initial stages of the phase transition. The blends were composed of model polyolefins—deuterium-labeled poly(methyl butylene) (PMB) and poly(ethyl butylene) (PEB)—with molecular weights of about 200 kg/mol. A direct examination of the initial clustering of molecules before macroscopic phase separation was possible because of the large size of the polymer chains and concomitant entanglement effects. We discovered that the scattering profiles obtained during nucleation merged at a well-defined critical scattering vector. We propose that this is the signature of the critical nucleus and that the size of the critical nucleus is inversely proportional to the magnitude of the critical scattering vector. The kinetic studies were preceded by a thorough characterization of the equilibrium thermodynamic properties of our PMB/PEB blends. The locations of the binodal and spinodal curves of our system are consistent with predictions based on the Flory–Huggins theory. This combination of thermodynamic and kinetic experiments enabled the quantification of the dependence of the size and structure of the critical nuclei on the quench depth. Our results do not agree with any of the previous theories on nucleation. Some aspects of our results are addressed in recent theoretical work by Wang in which the effects of fluctuations on the classical binodal and spinodal curves in polymer blends are incorporated. Both theory and experiment support the notion that the traditional stability limit (spinodal) should be replaced by a metastability limit. Although Wang's theory provides an explanation for some of our observations, many fundamental issues regarding nucleation in polymer blends remain unresolved. J Polym Sci Part B: Polym Phys 42: 1793–1809, 2004

Keywords: nucleation; phase separation; blends; neutron scattering; thermodynamics

Certain commercial equipment, instruments, or materials (or suppliers, or software) are identified in this article to foster understanding. Such identification does not imply recommendation or endorsement by the National Institute of Standards and Technology, nor does it imply that the materials or equipment identified are necessarily the best available for the purpose.

Correspondence to: N. P. Balsara (E-mail: nbalsara@cchem.berkeley.edu)

NITASH P. BALSARA

Nitash P. Balsara is a chemical engineer with a bachelors degree from the Indian Institute of Technology in Kanpur, India in 1982, a masters degree from Clarkson University in Potsdam, New York in 1984, and a PhD from Rensselaer Polytechnic Institute in Troy, New York in 1988. He did post-doctoral research at the Department of Chemical Engineering and Materials Science at the University of Minnesota, and at Exxon Research and Engineering Company in Annandale, New Jersey. In 1992, he joined the faculty of Department of Chemical Engineering at Polytechnic University in Brooklyn, New York. In 2000 he moved to the Department of Chemical Engineering at the University of California, Berkeley where he is currently a professor. His research is concerned with microstructure formation and phase transitions in multicomponent polymer materials.

TIMOTHY J. RAPPL

Timothy J. Rappl is a Ph.D. candidate in chemical engineering at the University of California, Berkeley working for Nitash Balsara towards an understanding of nucleation in polymer blends. He received his B.S. in chemical engineering from Rensselaer Polytechnic Institute in 2001.

AMY A. LEFEBVRE

Amy Lefebvre received her B.A. at Mount Holyoke College in 1992. She joined Nitash Balsara's group in 1996, where she studied phase separation in polymer blends. During the course of her studies she obtained her M.S. at Polytechnic University in 1999, and her Ph.D. in 2002 at the University of California Berkeley. In 2002, she joined the Atoglas Division of Atofina Chemicals as a scientist in the Product Development Group.

INTRODUCTION

Nucleation is a general term that describes the triggering of first-order phase transitions.[1–32] It is believed that different kinds of phase transitions, such as boiling, melting, crystallization, and phase separation, proceed by similar pathways because of the similarity of the underlying thermodynamic driving forces. Nucleation in some systems is entirely predictable. The crystallization of water is a typical example, ice forms at temperatures not

too far removed from its melting temperature. Nucleation in other systems is less predictable; the crystallization of polymers often requires the supercooling of the melt to temperatures as low as 50 °C below the melting temperature of the crystal. Polymer blends are similar in this respect; initiating phase separation requires substantial supercooling. The question of why nucleation occurs more readily in some systems and not in others remains unresolved because of both experimental and theoretical challenges.

The classical theories on this subject, dating back to the work of Gibbs,[1] assume that the nuclei formed during the initial stages of nucleation are composed of the final equilibrium phase with a well-defined interface. This immediately enables the calculation of the size of the smallest viable nucleus as long as the free energy difference between the initial and final phases and the interfacial energy are known. This is called the critical nucleus size (R_c). Within the classical framework, we thus expect to find small domains of the final equilibrium phase, with sizes greater than or equal to R_c, growing in the system. Most experimenters have not been able to probe the initial stages of nucleation. Instead, they have measured the rate of the phase transformation at later times and have inferred what must have happened during the initial stages of nucleation (e.g., ref. 4). Classical nucleation theory has provided an excellent framework for describing the results of such experiments. This has led to the belief that the assumptions of classical nucleation theory must have been satisfied during the initial stages.

The basic assumptions of classical nucleation theory have often been questioned. Ostwald, for example, indicated that phase transitions should proceed via the formation of nonequilibrium intermediate stages.[16,17] Addressing such effects require theories in which the order parameter of the nucleus is not constrained to be identical to that of the final equilibrium phase. For the case of liquid–liquid phase separation, such a theory was proposed many years ago by Cahn and Hilliard.[5] They obtained Gibbsian nuclei (with an order parameter similar to that of the final phase) at shallow quench depths in the vicinity of the binodal, and Ostwaldian nuclei (with an order parameter similar to that of the initial phase) at deep quench depths in the vicinity of the spinodal. At intermediate quench depths, a wide crossover regime was obtained, in which the characteristics of the critical nuclei changed gradually between the two extremes. We might thus expect to observe the formation of nonequilibrium structures during liquid–liquid phase separation, particularly at large quench depths.

It is perhaps appropriate to recognize that departures from conventional nucleation have been noted in recent studies of the initial stages of crystallization.[12–15,21–25] Theoretical studies of colloidal suspensions indicate that crystallization is facilitated by the presence of liquidlike, noncrystalline clusters.[12–15] The laser-induced nucleation of urea crystals, observed by Garetz et al.,[24] also suggests the existence of noncrystalline, intermediate states. The formation of mesomorphic nuclei has been proposed as a possible explanation for some of the anomalies observed during polymer crystallization.[25]

The main purpose of this article is to describe our attempts to study the initial stages of nucleation during liquid–liquid phase separation in polymer blends. We begin by describing experiments that probe the equilibrium properties of our system. We are particularly interested in determining the binodal and spinodal curves for our system because they set the boundaries within which nucleation is supposed to occur. We then present time-resolved small-angle neutron scattering (SANS) data obtained during the initial stages of liquid–liquid phase separation within these boundaries. We conclude by comparing our findings with available theories on nucleation.

Many textbooks on polymer physics[33–36] contain phase diagrams of polymer blends showing binodal and spinodal curves based on the Flory–Huggins theory. It is stated in these books that the mechanism of phase separation for blends located between the binodal and spinodal curves is nucleation and growth. The answer to the question posed in the title, "Does conventional nucleation occur during phase separation in polymer blends?", thus appears to be a foregone conclusion. We will demonstrate that this is not the case.

EXPERIMENTAL

We have studied blends of two model polyolefins, poly(methyl butylene) (PMB) and poly(ethyl butylene) (PEB). The PMB chains (PMB1 and PMB2) were labeled with deuterium, whereas the PEB chains (PEB1 and PEB2) were fully hydrogenous. The methods used to synthesize and characterize these polymers are described in refs. 37 and 38. The characteristics of the polymers are given in Table 1. Our molecules are much larger than the threshold for chain entanglement.[33,35] Binary PMB/PEB blends were made by methods described in ref. 37. The volume fractions of PMB in the blends used in this article are given in Table 2. These blends were studied by SANS experiments on the NG3 beam line at the National Institute of Standards and Technology (NIST; Gaithersburg, MD). The samples were housed in the NIST pressure cell; this enabled control over the sample temperature and pressure (at 30–200 °C and 0.03–3.10 kbar). The azimuthally averaged coherent scattering intensity (I) as a function of the scattering vector [$q = 4\pi\sin(\theta/$

Table 1. Characteristics of the Polymers

Polymer	Density (g/cm^3)	Average Number of Deuterium Atoms per 6 Carbon Atoms	Weight-Average Molecular Weight (g/mol)	Polydispersity Index	R_g (nm)
PMB1	0.9300	7.33	1.8×10^5	1.07	16.7
PMB2	0.9192	6.26	1.7×10^5	1.02	16.2
PEB1	0.8628	0	2.2×10^5	1.08	16.6
PEB2	0.8637	0	2.2×10^5	1.08	16.6

2)/λ, where θ is the scattering angle and λ is the wavelength of the incident neutron beam] was obtained by methods reported in ref. 37. Static SANS measurements enabled the determination of the binodal and spinodal curves.[37–40] Time-resolved SANS measurements enabled the determination of the size and other attributes of the growing nuclei as a function of the quench depth.[28–32] The experimental protocols used to study the three blends in Table 2 were similar, as were the results obtained from both the static and time-resolved SANS experiments. To avoid repetition, we thus often restrict our discussion to data obtained from one of the samples.

Most of the data presented in this article have appeared in a somewhat fragmented form in previous publications.[31,32,39–42] The main purpose of this article is to provide a comprehensive overview of our results on the subject of nucleation.

DETERMINATION OF BINODAL AND SPINODAL CURVES

The location of the binodal and spinodal, that is, the (T,P) values at which the homogeneous state is metastable and unstable, respectively, with respect to the phase-separated state, can be computed with the Flory–Huggins expression for the free energy density of mixing (ΔG_m) for a mixture of two homopolymers labeled 1 and 2:[43–45]

$$\frac{\Delta G_m}{kT} = \frac{\phi_1 \ln \phi_1}{v_1 N_1} + \frac{(1-\phi_1)\ln(1-\phi_1)}{v_2 N_2} + \frac{\chi \phi_1 (1-\phi_1)}{v_0} \quad (1)$$

Table 2. Blend Components and Compositions

Sample	Components A	Components B	ϕ_{PMB}
B1	PMB1	PEB1	0.161
B2	PMB1	PEB1	0.099
B3	PMB2	PEB2	0.160

where k is the Boltzmann constant, N_i is the number of monomer units in polymer chain i, ϕ_i is the volume fraction of polymer i, χ is the Flory–Huggins interaction parameter, v_i is the volume of monomer i, and v_0 is a reference volume (100 Å^3 in this work). χ, as defined in eq 1, contains contributions due to the internal energy change of mixing (ΔU) and the volume change of mixing (ΔV).[39–41]

The binodal curve, the curve that separates the one-phase and two-phase regions of the phase diagram, for a Flory–Huggins blend is calculated by the simultaneous solutions of the following two equations:

$$\ln\left(\frac{\phi_1^{\mathrm{I}}}{\phi_1^{\mathrm{II}}}\right) + (\phi_1^{\mathrm{II}} - \phi_1^{I})(1 - N_1 v_1 / N_2 v_2) + \frac{\chi(T,P) N_1 v_1}{v_0}[(1-\phi_1^{I})^2 - (1-\phi_1^{\mathrm{II}})^2] = 0 \quad (2)$$

$$\ln\left(\frac{1-\phi_1^{\mathrm{II}}}{1-\phi_1^{\mathrm{II}}}\right) + (\phi_1^{\mathrm{I}} - \phi_1^{\mathrm{II}})(1 - N_2 v_2 / N_1 v_1) + \frac{\chi(T,P) N_2 v_2}{v_0}[(\phi_1^{\mathrm{I}})^2 - (\phi_1^{\mathrm{II}})^2] = 0 \quad (3)$$

where ϕ_1^I and ϕ_1^{II} are the volume fractions of polymer 1 in the two coexisting phases labeled I and II, respectively. The spinodal curve, the limit of stability of the one-phase system, is given by

$$\frac{\partial^2(\Delta G/kT)}{\partial \phi_1^2} = \left(\frac{1}{N_1 v_1 \phi_1} + \frac{1}{N_2 v_2 \phi_2}\right) - 2\frac{\chi(T,P)}{v_0} = 0 \quad (4)$$

Equations 2–4 can be used to determine the binodal and spinodal curves if $\chi(T,P)$ is known.[46–48] We have obtained $\chi(T,P)$ from static SANS measurements with the random phase approximation (RPA) to interpret the data.[33] The q dependence of the typical static SANS intensity obtained from our blends is shown in Figure 1, in which we have plotted $1/I$ versus q^2 (Zimm plot) of blend B1 at selected temperatures at a fixed pressure of

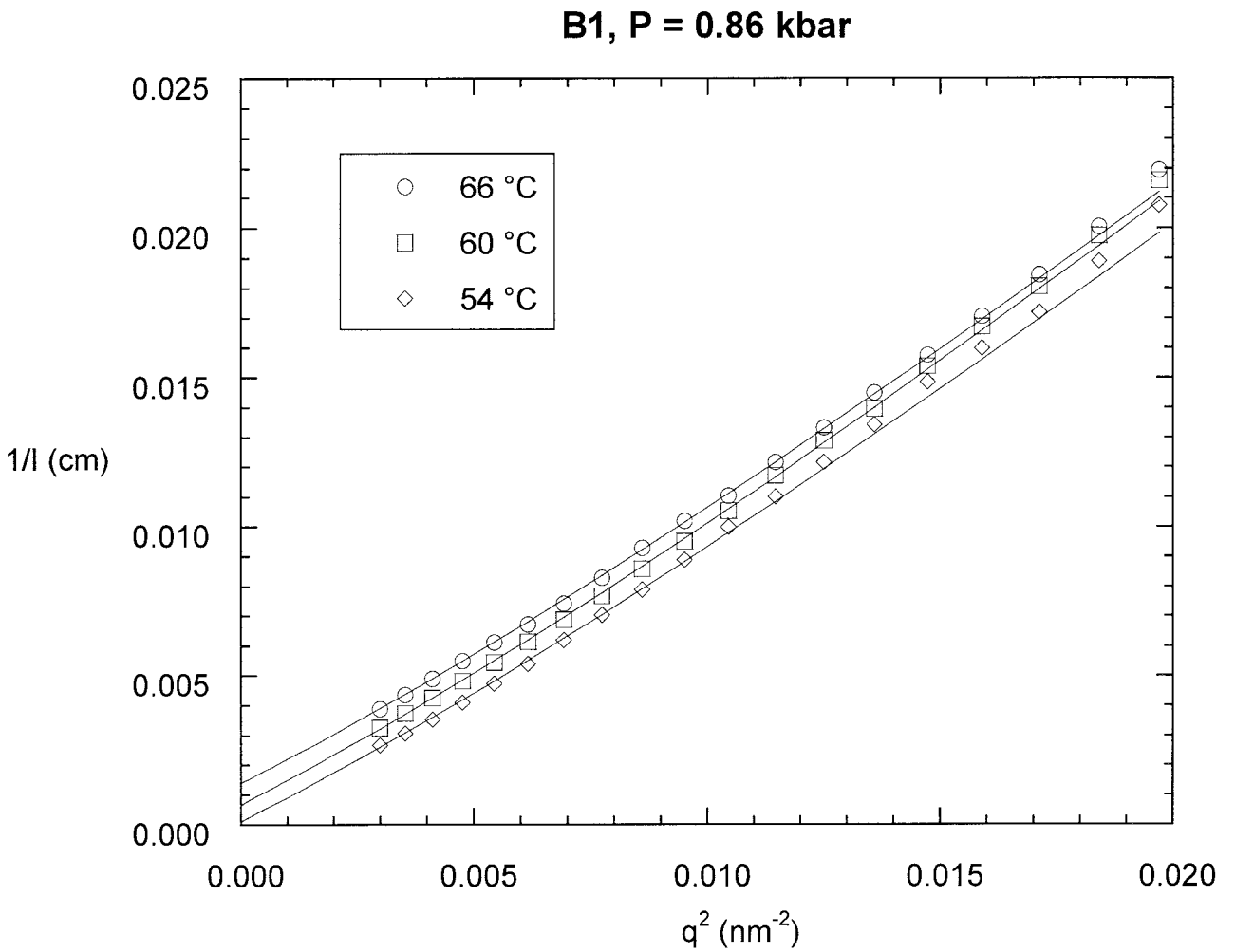

Figure 1. SANS intensity (I) for B1 at 0.86 kbar in the Zimm format ($1/I$ vs q^2). The curves through the data represent least-squares RPA fits. At 54 °C, $1/I$ is nearly zero, indicating the proximity of the blend to the spinodal.

0.86 kbar. The curves through the data in Figure 1 are least-squares RPA fits with χ as the main adjustable parameter.[49] The RPA captures all of the important features seen experimentally. In Figure 2, we show the temperature dependence of χ between PMB and PEB chains at 0.86 kbar, obtained by the fitting of the measured static SANS profiles of a variety of homogeneous blends, including B1, to the RPA. It is evident from Figure 2 that χ for PMB/PEB blends is independent of the blend composition and component molecular weights. This is an important simplification because the binodal and spinodal curves are given by eqs 2–4 only if χ is independent of the blend composition and component molecular weights. The phase diagram of blends B1 and B2 at 0.86 kbar thus obtained is shown in Figure 3. The vertical dashed lines indicate the temperature ranges over which the static SANS profiles from the blends were analyzed with the RPA. It is clear from Figure 3 that the RPA analysis was conducted both in the one-phase region and in the metastable two-phase region of the phase diagram. Slow nucleation, a fact that we will establish momentarily, is a crucial factor that enables the determination of χ at temperatures deep within the two-phase region of the phase diagram (Fig. 3). Obtaining the static SANS profiles from our blends requires data acquisition times of 5 min. It will be shown that the initiation of phase separation in PMB/PEB systems at these quench depths takes significantly longer than 5 min.

In Figure 4, we show the pressure dependence of the binodal temperature (T_b) and spinodal temperature (T_s), for blend B3, derived from the temperature and pressure dependence of χ. Before examining the initial stages of phase separation in our system, we must verify the location of the binodal and spinodal curves via independent experiments. It is customary to use the cloud-point method to locate the binodal curve.[50] This method as-

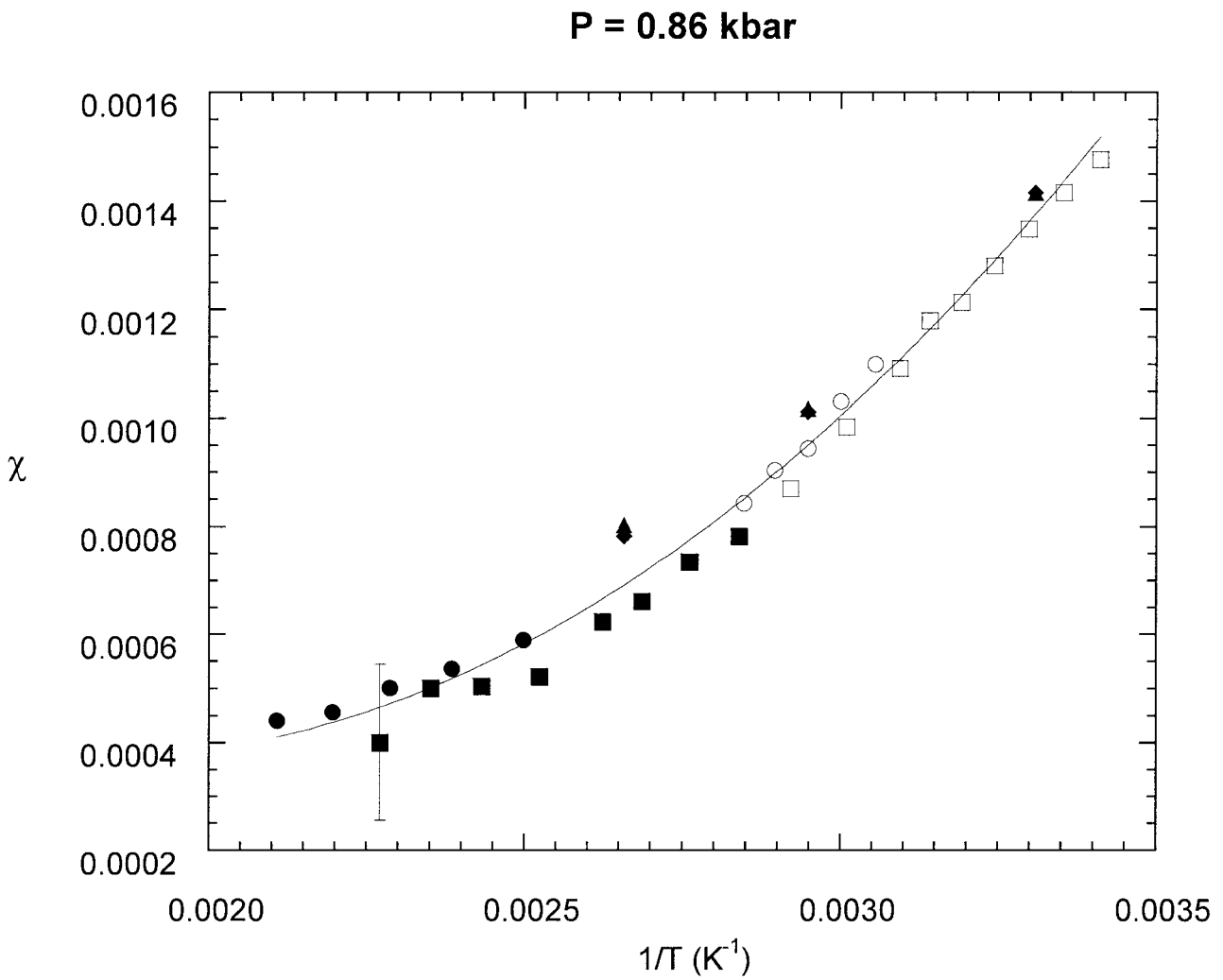

Figure 2. Dependence of χ on $1/T$ for PMB/PEB blends at 0.86 kbar. The circles represent B1, and the squares represent B2. The diamonds and triangles represent data from homogeneous blends with $\phi_{dPMB} = 0.414$ and $\phi_{dPMB} = 0.203$, respectively (see ref. 41 for details). The filled symbols indicate results from blends in the one-phase region. The unfilled symbols indicate results from blends in the metastable two-phase region. The error bar shows the largest error in χ. The curve is the least-squares quadratic fit through the data.

sumes that there are no nucleation barriers for liquid–liquid phase separation. This is an unreasonable assumption because the theoretically predicted nucleation barrier is proportional to $N^{1/2}$ (if both components have the same chain length N).[26,27] Our approach is to determine T_b at a given pressure by heating phase-separated samples and noting the temperature at which they become homogeneous. We assumed that our blends were homogeneous when the measured SANS profiles at given temperature and pressure values were close to predictions based on the RPA. The validity of this method rests on the assumption that the homogenization of polymer blends in the one-phase region is spontaneous. To minimize the importance of transport limitations for homogenization, we studied samples that had been aged in the two-phase region of the phase diagram for relatively little time. The homogenization experiment was started before the onset of the late stage of phase separation, that is, before the formation of large domains separated by sharp interfaces was observed. The circles in Figure 4 show the homogenization temperatures of sample B3 obtained at different pressures. We find quantitative agreement between the homogenization temperatures and the Flory–Huggins binodal curve (Fig. 4).

The verification of the location of the spinodal of blend B1 is shown in Figure 1. The proximity of blend B1 to the

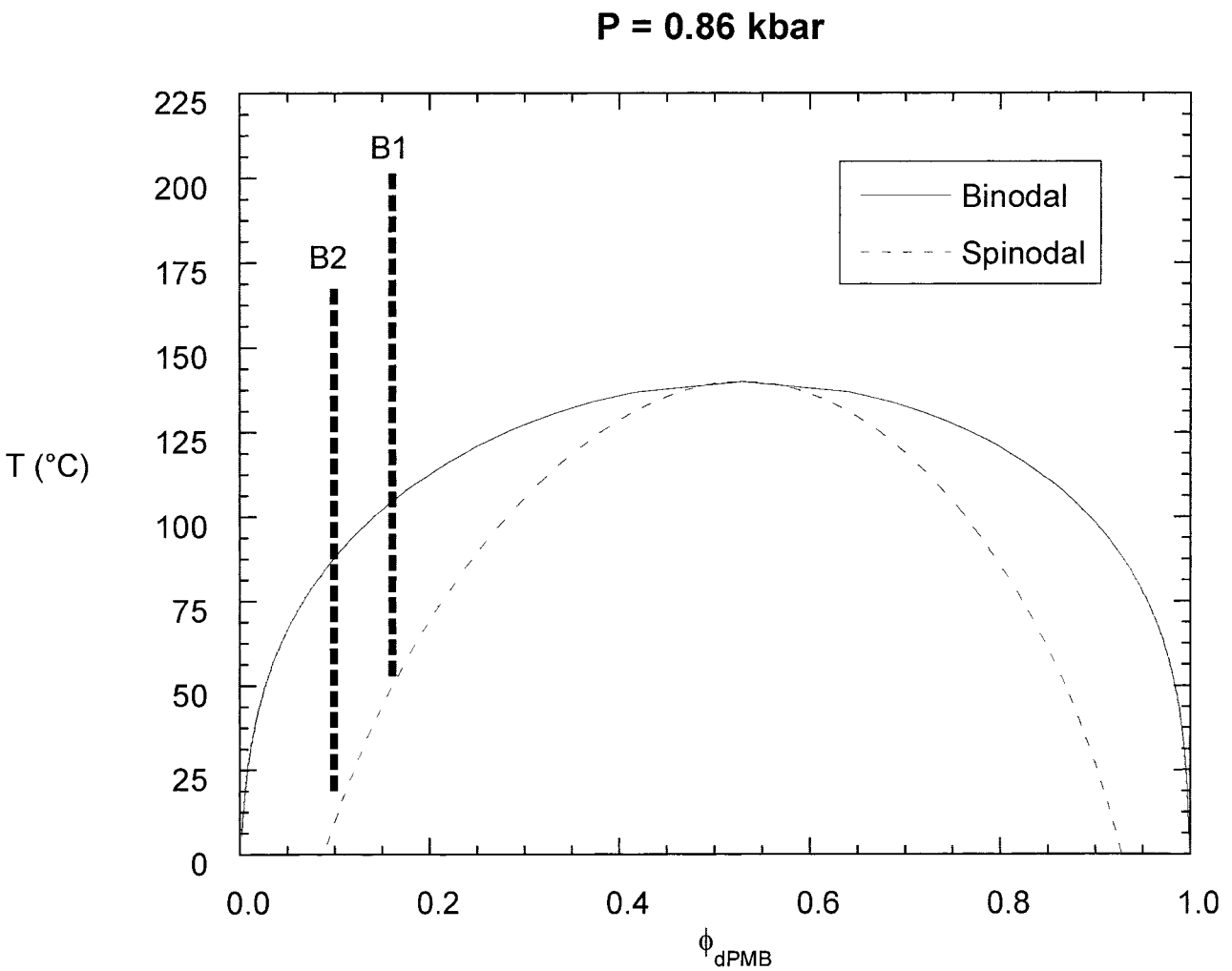

Figure 3. Calculated phase diagram for blends B1 and B2 at 0.86 kbar in a temperature-versus-ϕ_{dPMB} format. The solid curve is the binodal curve, and the thin dashed curve is the spinodal curve. The vertical dashed lines show the range over which χ values were determined for B1 and B2.

spinodal at lower temperatures is clear from the fact that the extrapolated intensity as q approaches 0 is very large. We use the RPA to extrapolate the scattering data to obtain $I(q \rightarrow 0)$, as indicated in Figure 1. At 54 °C, $I(q \rightarrow 0)$ is 10^4 cm^{-1}, and the sample is estimated to be 4 °C from the theoretical T_s value based on the Flory–Huggins theory. Attempts to obtain the structure factor of the metastable state of B1 at temperatures below 54 °C (0.86 kbar) failed because of rapid phase separation. It is clear from Figure 1 that we have identified T_s of our off-critical blend with an accuracy of about 5 °C.

This sets the stage for examining the initial stages of phase separation in our samples. The location of the quenches conducted on blend B3 are represented by squares in the phase diagram (Fig. 4). Because of our interest in nucleation, most of our quenches were located in the metastable region between the binodal and spinodal curves. Details regarding the procedures used to quench the sample are given in ref. 31.

INITIAL STAGES OF PHASE SEPARATION

Typical SANS profiles obtained after the quenching of our samples are shown in Figure 5, in which we show data obtained from B3 for selected quenches. At large quench depths (at 3.10 kbar), we see a rapid increase in the absolute scattering intensity [$I(q)$], particularly at low q values, which indicates the growth of structures with large length scales. As the quench depth decreases, phase separation becomes slower. For example, I at the lowest accessible q value (0.021 nm^{-1}) increases by a factor of

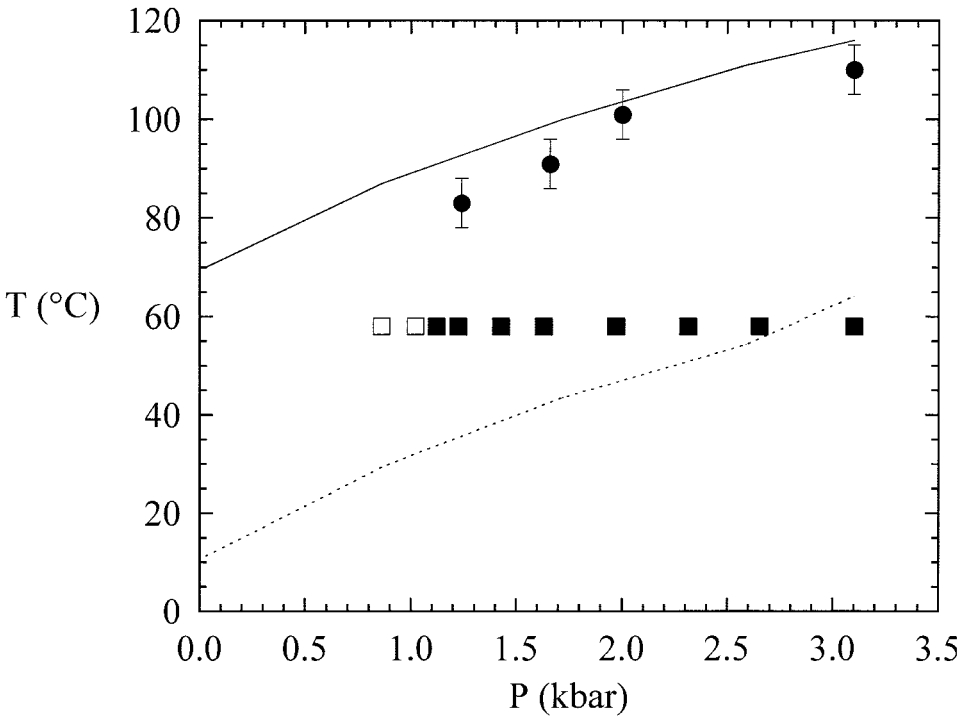

Figure 4. Calculated phase diagram for blend B3 at $\phi_{dPMB} = 0.16$ in a temperature-versus-pressure format. The solid curve represents the pressure dependence of T_b, and the dashed curve represents the pressure dependence of T_s, both calculated from the Flory–Huggins theory. The filled circles represent experimentally determined T_b's. The locations of the quenches studied during phase-separation experiments are represented as squares. The closed squares represent quenches that led to phase separation; the open squares represent quenches that did not lead to phase separation.

2 in 70 min at 3.10 kbar, whereas at 1.24 kbar, the same increase is seen in 230 min. At 0.86 kbar, which is between the binodal and the spinodal of our blend [Fig. 5(d)], we see no evidence of phase separation.

In Figure 6(a), we show the time dependence of I(q $= 0.021$ nm^{-1}) after the quenching of blend B3 at 58 °C and 2.31 kbar. We see two regimes of behavior: an early stage ($t < 150$ min) in which the growth of I was slow and a late stage ($t > 150$ min) in which the growth of I was rapid. In systems with significant nucleation barriers, we expect a slow nucleation process followed by a rapid growth process. We define time τ_E to be the time required to complete the early stage of phase separation. The numerical procedure used to determine τ_E from the data is given in ref. 31. The dependence of τ_E on the quench depth for all three blends is given in Figure 6(b). The abscissa in Figure 6(b) is χ/χ_s, where χ is the Flory–Huggins interaction parameter at the temperature and pressure values at which the phase-separation experiments were carried out and χ_s is the value of χ at the spinodal at the same temperature and pressure (eq 4). Figure 6(b) shows that τ_E decreases rapidly as the spinodal is approached. This is expected if what occurred in our blends at times less than τ_E was nucleation. Nucleation is an activated process, and the time required to cross the nucleation barrier is directly dependent on the height of the barrier. According to the classical view, the barrier for nucleation disappears at the spinodal. This would imply that the timescale required for nucleation should approach molecular relaxation timescales at the spinodal (i.e., $\chi/\chi_s = 1$). The data in Figure 6(b) are thus in qualitative agreement with expectations based on classical nucleation theory.

Figure 6 describes the evolution of the SANS intensity at small scattering vectors. It is clear from Figure 5 that the rate of growth of the SANS intensity is a strong function of the quench depth and q. At a given quench depth, we find that the SANS intensity over a range of scattering vectors is, in fact, independent of time. We use the term q_c (the critical scattering vector) to denote the low q limit of this range of scattering vectors. Numerical procedures to identify q_c are described in ref. 31, and the results of this analysis are shown in the insets of Figure 5(a–c). Because the value of the scattering intensity at q is indicative of the growth of structures with a characteristic length of 1/q (within a constant), $1/q_c$ represents

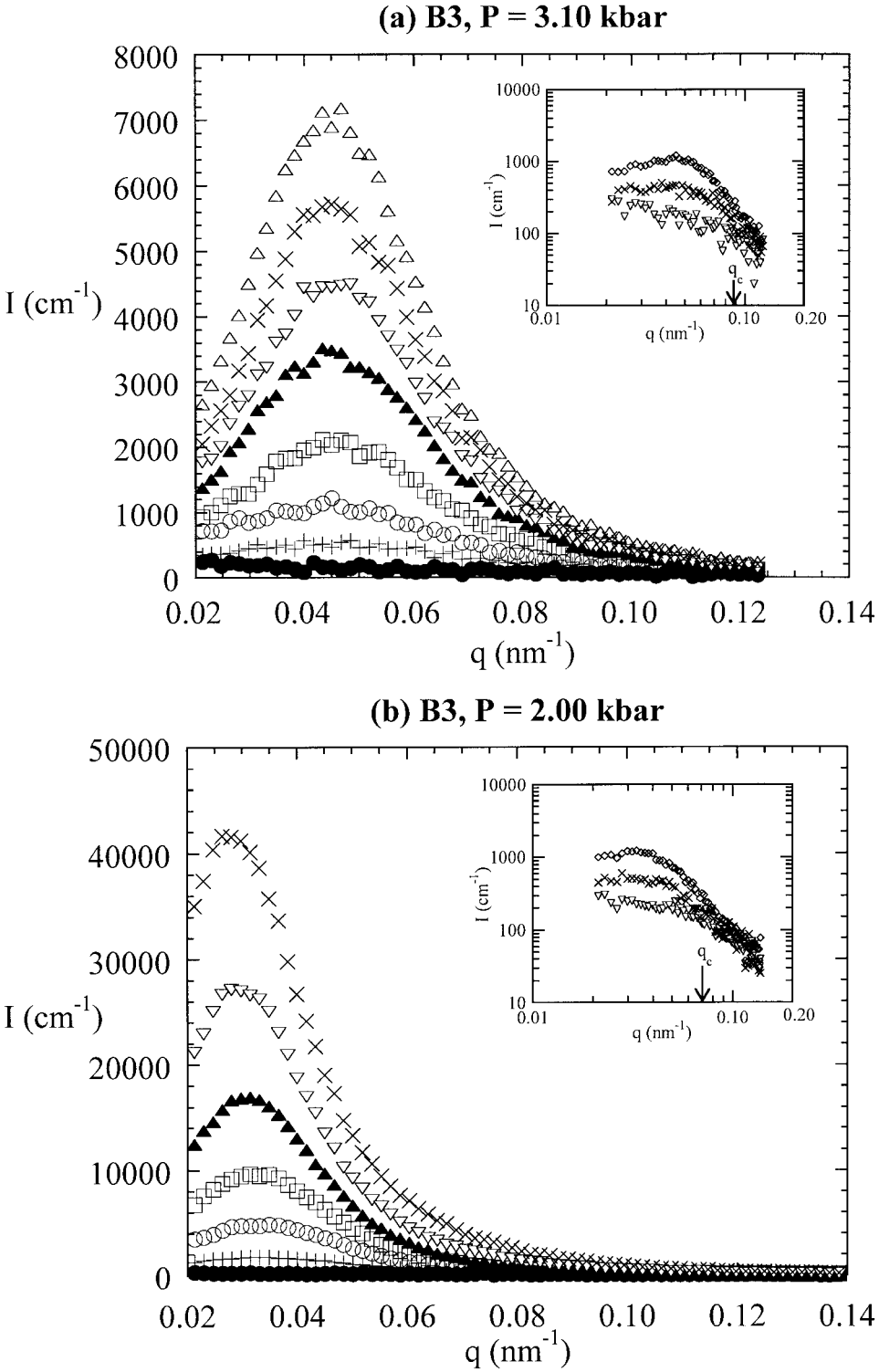

Figure 5. Time dependence of scattering intensity, *I,* versus scattering vector, q, for the B3 blend during phase separation at 58 °C and (a) 3.10, (b) 2.00, (c) 1.24, and (d) 0.86 kbar. From small to large intensities, the SANS profiles are for times: (a) 3, 77, 141, 189, 231, 252, 273, and 294 min; (b) 3, 153, 211, 253, 295, 337, and 379 min; and (c) 3, 475, 569, 694, 788, and 945 min. The inserts show log–log plots of $I(q)$ versus q. From small to large intensities, the SANS profiles are for times: (a) 5, 64, and 141 min; (b) 6, 58, and 130 min; and (c) 3, 54, 412, 538, and 663 min. The arrows indicate the locations of the critical scattering vectors, q_c.[31]

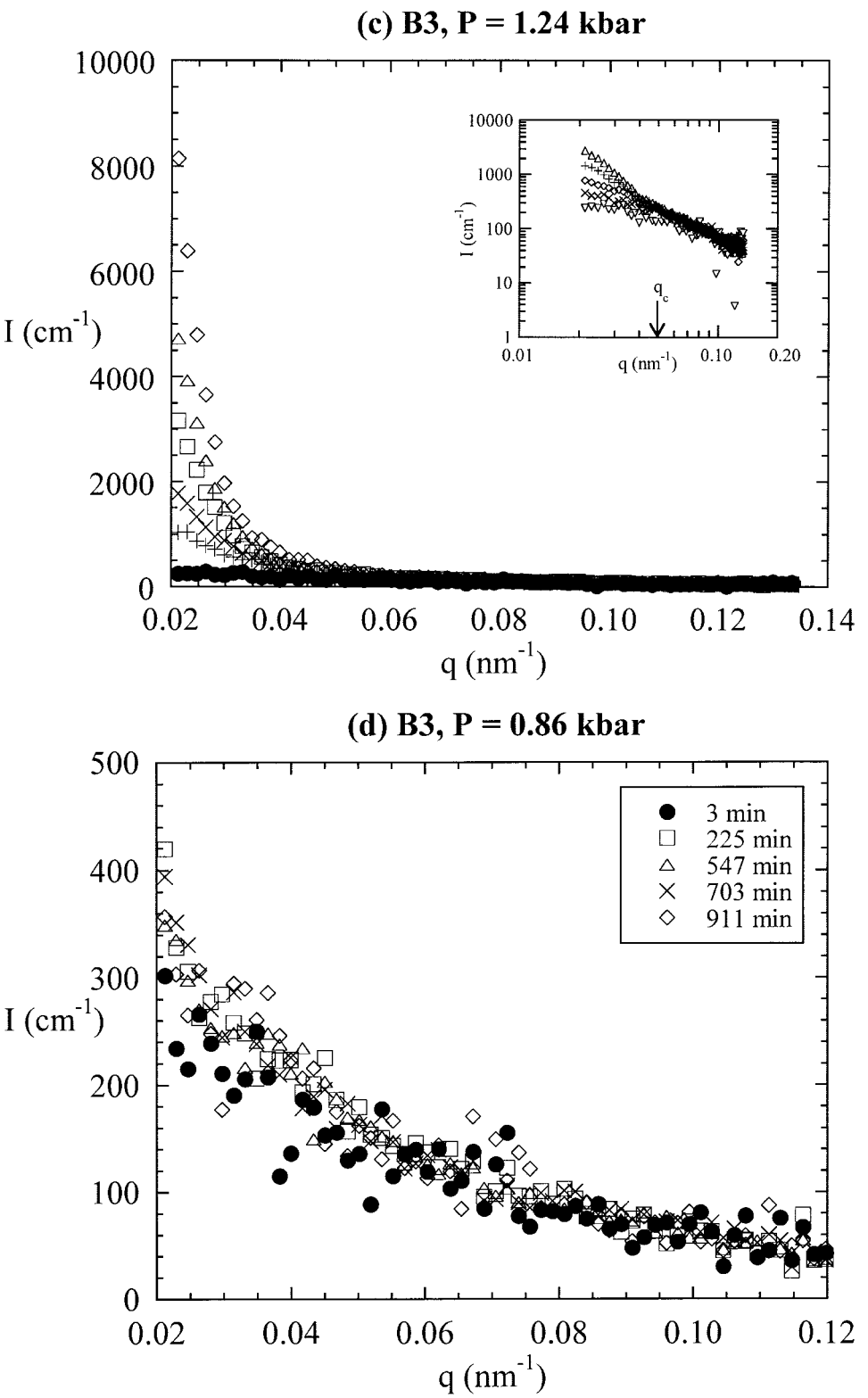

Figure 5. *(Continued from the previous page)*

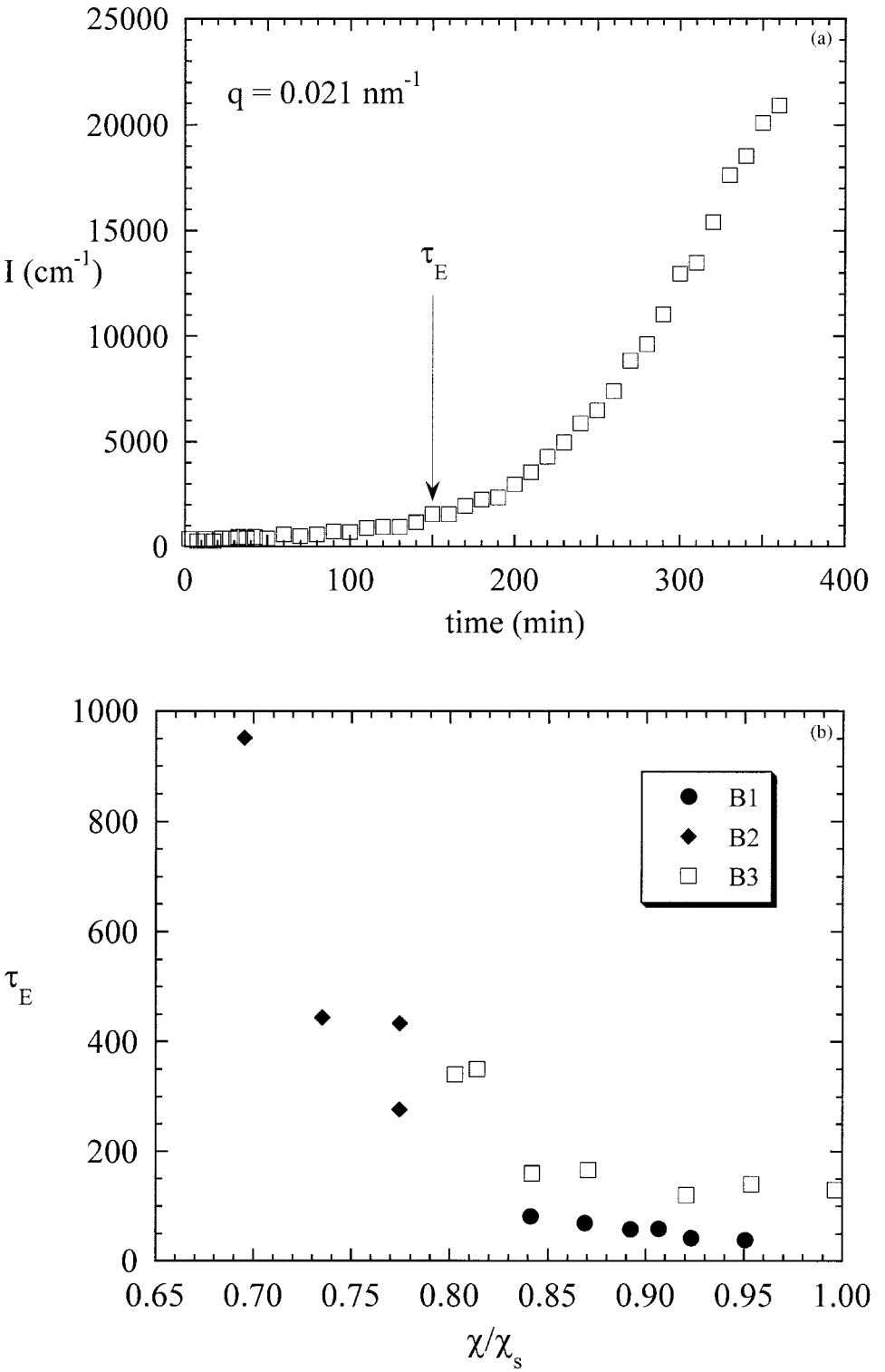

Figure 6. (a) I versus time at q = 0.021 nm^{-1} for blend B3 at 2.31 kbar. The arrow shows the location of τ_E. (b) Quench depth dependence of τ_E for blends B1, B2, and B3. The quench depth is represented as χ/χ_s. The two data points for blend B2 at χ/χ_s = 0.775 were obtained from different blend samples of the same composition. The difference between the two τ_E values provides an estimate of the error in the measurements.

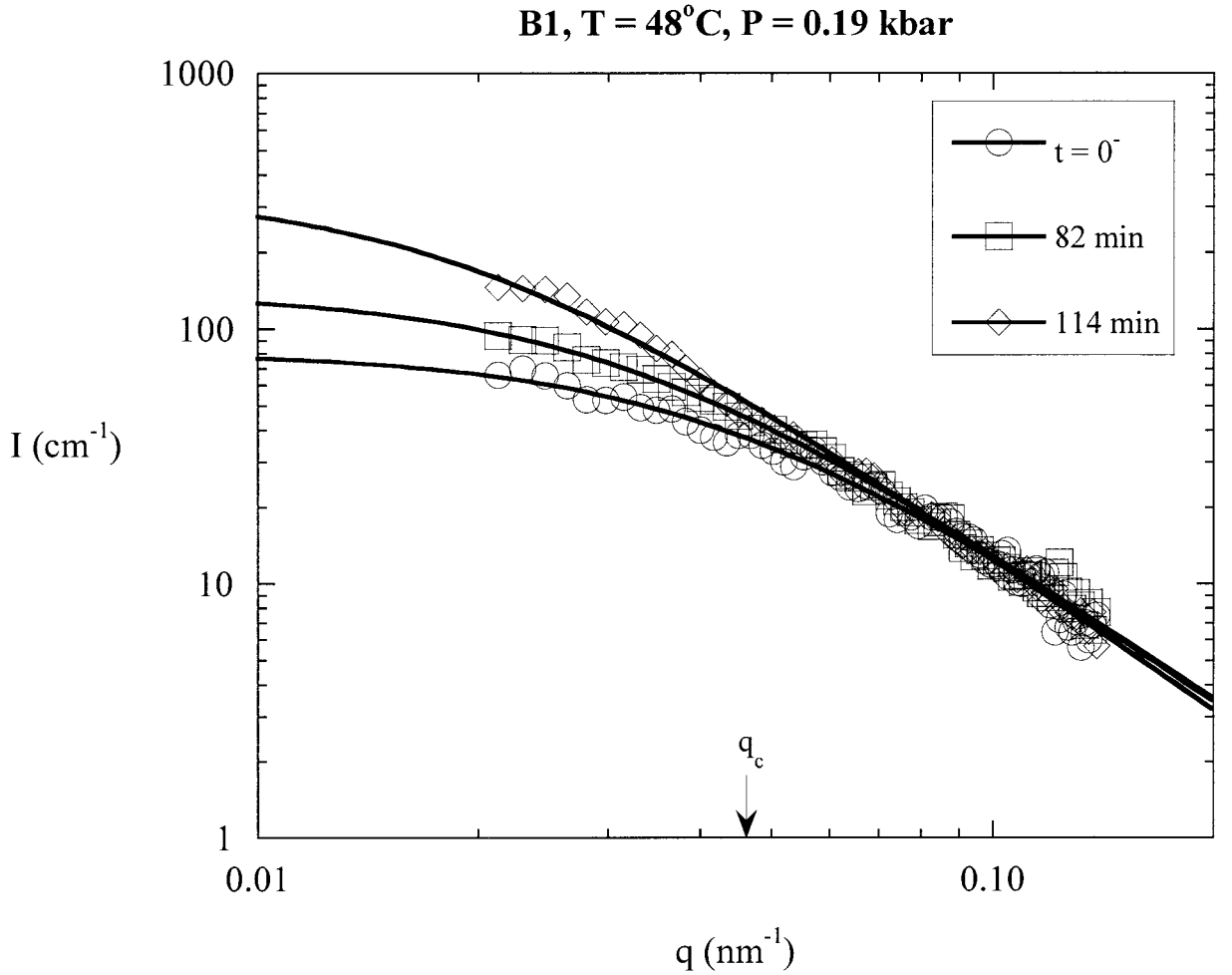

Figure 7. I versus q for blend B1 at 48 °C and 0.19 kbar. The solid lines represent least-squares fits of the OZ equation. The location of q_c is represented by an arrow.

a lower bound for the length scale of the growing structures. This is precisely the definition of R_c in conventional nucleation theories. We thus propose that R_c is simply given by

$$R_c = k/q_c \tag{5}$$

where k is a numerical prefactor that depends on the shape and content of the growing nuclei. Because we have not yet determined all of the characteristics of the growing nuclei, we cannot assert what k is.

The SANS profiles obtained during the early stage of phase separation are consistent with the Ornstein–Zernicke (OZ) equation. This is shown in Figure 7, in which we show data obtained from sample B1 during the early stage of phase separation. The curves through the data are least-squares fits of the OZ equation:

$$I(\mathrm{q}) = \frac{I_0}{1 + \mathrm{q}^2\xi^2} \tag{6}$$

where ξ is the characteristic length of the structures in the sample and I_0 is related to the average scattering power of the structures. The OZ equation is usually used to describe the buildup of concentration fluctuations as the critical point is approached in the mean-field limit, in which case one obtains $I_0 \sim \xi^{1/2}$. OZ fits through the time-dependent SANS data from our samples enable the determination of the time dependence of I_0 and ξ.[51] In Figure 8, we have plotted I_0 versus ξ obtained from samples B1 and B2 normalized by the values of these parameters at $t = 0$. The collapse of the data indicates that the structures that grow in the early stages of phase separation are self-similar. This self-similarity is not consistent with the Cahn–Hilliard theory of nucleation, in which the nuclei are predicted to become increasingly diffuse as the spinodal is approached. The experimentally determined exponent for I_0-versus-ξ scaling is 0.58 $\pm$ 0.04, which is not very different from 0.5, the exponent for mean-field concentration fluctuations. We thus conclude that the structures formed during the early

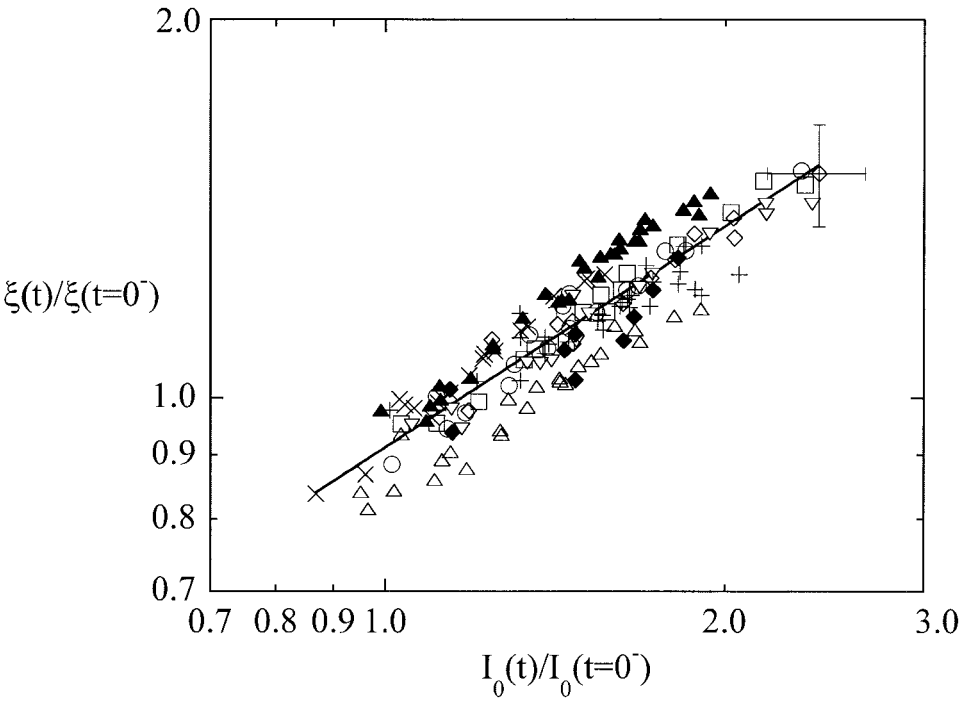

Figure 8. Dependence of the OZ parameters, ξ versus I_0 (obtained at the same time), during the early stages of nucleation and normalized by their prequench values. Both I_0 and ξ increase monotonically with time (see ref. 30 for details). The pressures for sample B1 were (+) 0.19, (○) 0.27, (□) 0.34, (▽) 0.38, (◇) 0.43, and (◆) 0.51 kbar. The temperatures for sample B2 were (▲) 40 and (+,△) 35 °C (two separate quenches). The solid line is the least-squares power law fit through the data. The error bars indicate average uncertainty in the parameters.

stages of phase separation are diffuse and qualitatively similar to concentration fluctuations found in homogeneous mixtures. It is important to note that compact Gibbsian structures, predicted by classical nucleation theory, would neither be described by the OZ equation nor give the observed I_0-versus-ξ scaling. The observed self-similarity implies that prefactor k in eq 5 is independent of the quench depth.

The dependence of R_c on the quench depth is shown in Figure 9, in which $(R_g/R_c)^2$ is plotted as a function of χ/χ_s for all three blends. For convenience, we have set the prefactor k in eq 5 to unity and normalized the measured R_c values by R_g, the radius of gyration of the homopolymers used in this work, which equals 16 ± 1 nm. The theoretical expression for the dependence of $(R_g/R_c)^2$ on χ/χ_s obtained by Cahn and Hilliard[5] is

$$\left(\frac{R_g}{R_c}\right)^2 = \left(\frac{2\chi N}{0.73}\right)^2 \phi(1-\phi)\left(\frac{1}{2} - \frac{1}{2}\sqrt{1-\frac{2}{\chi N}} - \phi\right) \times \left(\sqrt{1-\frac{2}{\chi N}}\right)(\chi/\chi_s < 1) \quad (7)$$

For completeness, we also show the dependence of $(R_g/R_c)^2$ on χ/χ_s obtained by Cahn[52] for quenches inside the spinodal:

$$\left(\frac{R_g}{R_c}\right)^2 = 3\left(\frac{\chi}{\chi_s} - 1\right)(\chi/\chi > 1) \quad (8)$$

The curves in Figure 9 are the theoretical prediction for the dependence of $(R_g/R_c)^2$ on the quench depth with eqs 7 and 8. It is evident that the Cahn–Hilliard theory predicts that R_c increases with increasing quench depth in the nucleation regime ($\chi/\chi_s < 1$) and that it diverges at the spinodal. In contrast, our experiments indicate that R_c decreases smoothly with increasing quench depth. We also see no evidence for the nonanalytical dependence of R_c on the quench depth in the vicinity of the spinodal (Fig. 9).

The previously described phase-separation kinetics (Figs. 5–9) are not consistent with any known theory of spinodal decomposition or nucleation and growth. This was one of the factors that motivated Wang and coworkers[26,27] to reevaluate the applicability of the mean-field

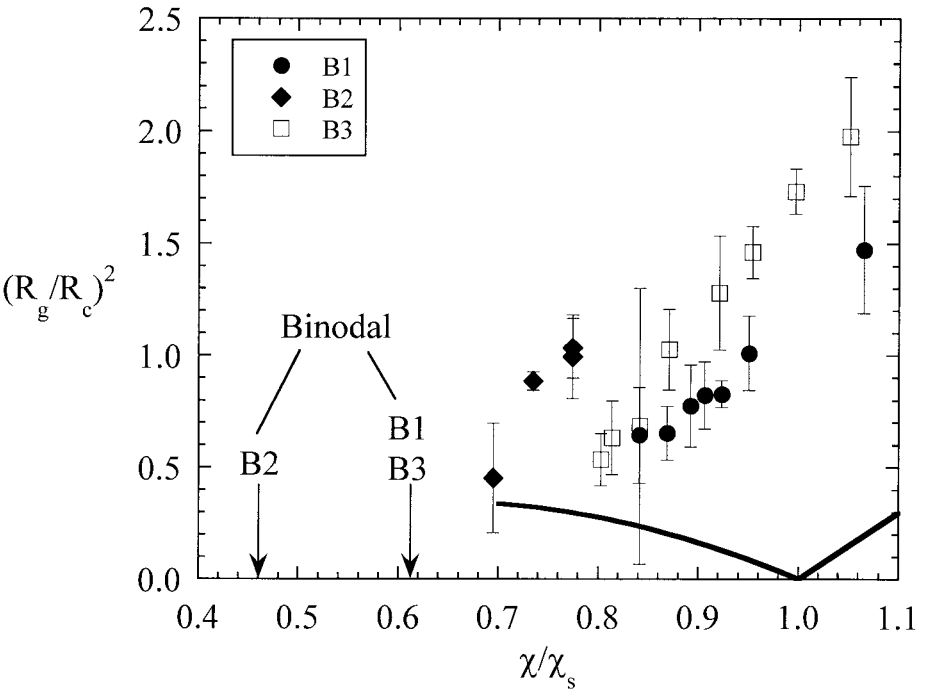

Figure 9. Plot of $(R_g/R_c)^2$ versus the quench depth (χ/χ_s) for blends B1, B2, and B3. The error bars in $(R_g/R_c)^2$ are due to uncertainties in the location of q_c. The solid curve is the theoretical prediction for blend B2 (eqs 7 and 8). The arrows indicate the values of χ/χ_s at the binodal for the three blends.

theory of polymer blends. This new theory indicates that polymer blends with $N = 3000$ (the range of N values in our experiments) cannot be treated as mean-field systems. It is thus necessary to correct the mean-field theory for the presence of concentration fluctuations. A new theory, in which the effects of concentration fluctuations on thermodynamics are treated perturbatively, has been developed and used to characterize the nature of concentration fluctuations in single-phase, metastable blends. Not surprisingly, it was found that the binodal fluctuations grew in magnitude with increasing quench depth (i.e., increasing χ). This behavior was, however, restricted to $\chi \leq \chi_m$. χ_m is given by the following analytical expression:

$$\chi_{ml} = \chi_s \left\{ 1 - 2.5 \left(\frac{l_1 l_2}{\bar{l}} \right) \frac{(V_1 V_2)^{1/3}}{\bar{V}} \times \left[\frac{((1-\phi_1)^2 V_2 - \phi_1^2 V_1)^2}{\phi_1 (1-\phi_1) V_1 V_2} \right]^{2/3} \right\} \quad (9)$$

where V_i is equal to $N_i v_i$, l_i is equal to V_i/R_i^2, $\bar{V}$ is equal to $\phi_1 V_1 + (1-\phi_1)V_2$, $\bar{l}$ is equal to $\phi_1 l_1 + (1-\phi_1) l_2$, and R_i is the end-to-end distance of polymer i and is given by $R_i^2 = N_i l_{si}^2$ (where l_{si} is the statistical segment length of polymer i). In the regime $\chi > \chi_m$, the theoretically obtained concentration fluctuations decay with increasing quench depth. This unphysical result is obtained because the magnitude of the fluctuation corrections at $\chi > \chi_m$ are so large that the perturbative approximations used to obtain the theoretical result break down. Wang argued that in the presence of such large fluctuations, it would be impossible to maintain the metastable one-phase state and thus phase separation at these quench depths would be spontaneous. He thus called χ_m the limit of metastability. This limit is entirely analogous to the breakdown of a mean-field theory at the stability limit, that is, at the spinodal. Additionally, the nucleation barriers in the vicinity of χ_m are approximately kT. Therefore, it is difficult to distinguish between nucleation and growth and spinodal decomposition in this regime. The existence of such a regime was first postulated by Binder.[9,11]

Figure 10 shows the mean-field binodal and spinodal curves on a χN-versus-ϕ_{PMB} plot.[53] The predicted location of the fluctuation-corrected metastability limit obtained with eq 9 is also shown. The symbols in Figure 10 represent the location of the quenches that were conducted on sample B3. The filled symbols indicate the locations of quenches that resulted in observable phase separation, whereas the unfilled symbols indicate the locations of the quenches that did not result in phase

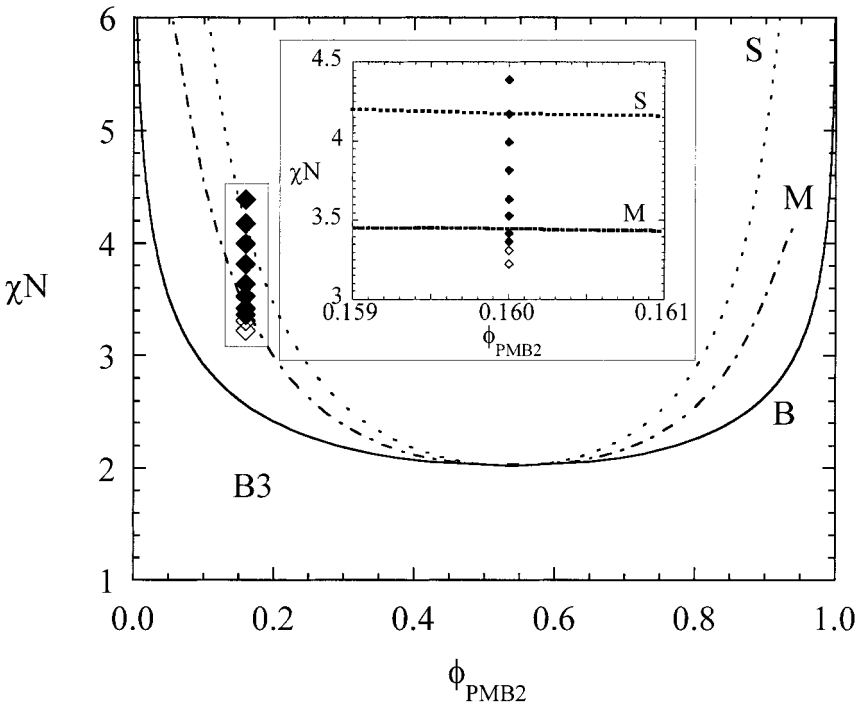

Figure 10. Calculated χN-versus-ϕ_{dPMB} phase diagram for blend B3 (see ref. 52 for details). The solid curve (B) is the mean-field binodal curve, the dashed curve (S) is the mean-field spinodal curve, and the dotted–dashed curve (M) is the metastability limit proposed by Wang.[27] The values of χN at which phase separation was observed and was not observed are indicated by filled and open diamonds, respectively. The inset shows an expanded view of the theory and experimental data near the metastability limit.

separation. The quench depth at which we see these two qualitatively different behaviors is $\chi/\chi_s = 0.796 \pm 0.007$ (or $\chi N = 3.25$). The theoretical limit of metastability for blend B3 is $\chi/\chi_s = 0.831$ (or $\chi N = 3.40$). The agreement between the experimental and theoretical limits of metastability is remarkable given the uncertainties in χ and the fact that the agreement is obtained without any adjustable parameters.

Although Wang's theory provides an explanation for some of our observations, many fundamental issues regarding nucleation remain unresolved. The theory predicts that the concentration fluctuations near the metastability limit are very different from the mean-field predictions. If this were true, then χ obtained through the fitting of the static SANS profiles in this regime would be substantially different from predictions based on the mean-field theory (RPA). In contrast, the data in Figures 1 and 2 show that the static SANS profiles of our blends are in complete agreement with the mean-field theory. Wang's theory also provides no explanation for the self-similarity of the structures seen during the early stages of phase separation (Fig. 8) or the observed dependence of R_c on the quench depth (Fig. 9). Perhaps we can resolve these issues by studying the dynamic consequences of the fluctuation corrections proposed by Wang.

CONCLUSIONS

We have completed a comprehensive study of the equilibrium and nonequilibrium thermodynamic properties of off-critical, high-molecular-weight polymer blends with static and time-resolved SANS. Our objective was to observe the formation of critical nuclei during the initial stages of liquid–liquid phase separation. Previous studies on the initial stages of liquid–liquid phase separation in polymer blends have focused on critical blends undergoing spinodal decomposition.[54–58] We chose the PMB/PEB blend system because χ for this system is independent of the blend composition and molecular weight (Figs. 1 and 2). We could thus assume that the equilibrium thermodynamic properties of our blends were given by the Flory–Huggins theory. We found good agreement between the binodal (Fig. 4) and spinodal (Figs. 1 and 3) curves obtained from theory and experiment. We then studied the kinetics of phase separation, focusing on quenches into the metastable region of the phase diagram bounded by the binodal and spinodal curves.

We have established that the scattering from structures formed during the initial stages of phase separation is consistent with the OZ equation (Fig. 7). The OZ parameters obtained from all of the blends obey a uni-

versal scaling law (Fig. 8), indicating that structures responsible for nucleation are diffuse and self-similar and that their characteristics are independent of the quench depth. We found that the scattering profiles obtained during phase separation were independent of time for q values greater than q_c. We concluded that the growing structures during the initial stages of nucleation must have length scales greater than $1/q_c$. The lower limit of the length scale of the structures responsible for the initial phase-separation process, R_c, is thus equal to $1/q_c$. We found that R_c decreased monotonically with increasing quench depth. A major prediction of conventional nucleation theories is the divergence of R_c at the spinodal. We found no evidence of such a divergence. We thus conclude that the spinodal, defined as the quench depth at which the static structure factor of a mixture diverges, appears to have no dynamic significance. Recent theories of Wang and coworkers[26,27] have shown that fluctuation corrections to the mean-field theory of polymer blends naturally lead to the existence of a metastability limit. Experimentally, we have observed that phase separation can only be initiated in our blends when the quench depth exceeds a particular critical value. The theoretically predicted metastability limit and the experimentally obtained critical quench depth are in reasonable agreement (Fig. 10).

Our work indicates that the nucleation pathways in polymer blends are not consistent with any of the available theoretical predictions. The answer to the question, "Does conventional nucleation occur during phase separation in polymer blends?", is, therefore, "No".

The authors acknowledge the donors of the Petroleum Research Fund (administered by the American Chemical Society), the Polymer Program of the Materials Sciences Division of Lawrence Berkeley National Laboratory (U.S. Department of Energy), and the National Science Foundation (CTS-305711) for their support of this research. The authors also acknowledge the support of the National Institute of Standards and Technology (U.S. Department of Commerce) in providing the facilities used in this work. The small-angle neutron scattering instrument was supported by a grant (DMR-9986442) from the National Science Foundation to the National Institute of Standards and Technology. Educational discussions and experimental help of Boualen Hammouda are gratefully acknowledged.

REFERENCES AND NOTES

1. Gibbs, J. W. The Scientific Papers of J. Willard Gibbs; Dover: New York, 1961.
2. Becker, R.; Doring, W. Ann Phys (Leipzig) 1935, 24, 719.
3. Gunton, J. D.; San Miguel, M. Sahani in Phase Transitions; Academic: New York, 1983; Vol. 8.
4. Debenedetti, P. G. Metastable Liquids Concepts and Principles; Princeton University Press: Princeton, NJ, 1996.
5. Cahn, J. W.; Hilliard, J. E. J Chem Phys 1959, 31, 688.
6. Binder, K.; Stauffer, D. Adv Phys 1976, 25, 343.
7. Sur, A.; Lebowitz, J. L.; Marro, J.; Kalos, M. H. Phys Rev B 1977, 15, 3014.
8. Langer, J. S.; Schwartz, A. J. Phys Rev A 1980, 21, 948.
9. Binder, K. J Chem Phys 1983, 79, 6387.
10. Heermann, D. W.; Klein, W. Phys Rev B 1983, 27, 1732.
11. Binder, K. Phys Rev A 1984, 29, 341.
12. ten Wolde, P. R.; Frenkel, D. Science 1997, 277, 1975.
13. Talanquer, V.; Oxtoby, D. W. J Chem Phys 1998, 109, 223.
14. Oxtoby, D. W. Acc Chem Res 1998, 31, 91.
15. Shore, J. D.; Perchak, D.; Shnidman, Y. J Chem Phys 2000, 113, 6276.
16. Schmelzer, J. W. P.; Schmelzer, J.; Gutzow, I. S. J Chem Phys 2000, 112, 3820.
17. Ostwald, W. Z Phys Chem Stoechiom Verwandtschadtsl 1897, 22, 289.
18. Wong, N. C.; Knobler, C. M. J Chem Phys 1978, 69, 725.
19. Howland, R. G.; Wong, N. C.; Knobler, C. M. J Chem Phys 1980, 73, 522.
20. Krishnamurthy, S.; Goldburg, W. I. Phys Rev A 1980, 22, 2147.
21. Schätzel, K.; Ackerson, B. J. Phys Rev E 1993, 48, 3766.
22. Yau, S.-T.; Vekilov, P. G. Nature 2000, 406, 494.
23. Gasser, U.; Weeks, E. R.; Schofield, A.; Pusey, P. N.; Weitz, D. A. Science 2001, 292, 258.
24. Garetz, B. A.; Aber, J. E.; Goddard, N. L.; Young, R. G.; Myerson, A. S. Phys Rev Lett 1996, 77, 3475.
25. Strobl, G. Eur Phys J E 2000, 3, 165
26. Wood, S. M.; Wang, Z.-G. J Chem Phys 2002, 116, 2289.
27. Wang, Z.-G. J Chem Phys 2002, 117, 481.
28. Balsara, N. P.; Lin, C. C.; Hammouda, B. Phys Rev Lett 1996, 77, 3847.
29. Lefebvre, A. A.; Lee, J. H.; Jeon, H. S.; Balsara, N. P. J Chem Phys 1999, 111, 6082.
30. Lefebvre, A. A.; Lee, J. H.; Balsara, N. P.; Hammouda, B. J Chem Phys 2002, 116, 4777.
31. Lefebvre, A. A.; Lee, J. H.; Balsara, N. P.; Vaidyanathan, C. J Chem Phys 2002, 117, 9063.
32. Lefebvre, A. A.; Lee, J. H.; Balsara, N. P.; Vaidyanathan, C. J Chem Phys 2002, 117, 9074.
33. de Gennes, P. G. Scaling Concepts in Polymer Physics; Cornell University Press: Ithaca, NY, 1979.

34. Higgins, J. S.; Benoît, H. C. Polymers and Neutron Scattering; Oxford University Press: New York, 1994.
35. Doi, M. Introduction to Polymer Physics; Oxford University Press: New York, 1996.
36. Strobl, G. The Physics of Polymers: Concepts for Understanding Their Structure and Behavior; Springer-Verlag: New York, 1997.
37. Balsara, N. P.; Jonnalagadda, S. V.; Lin, C. C.; Han, C. C.; Krishnamoorti, R. J Chem Phys 1993, 99, 10011.
38. Lin, C. C.; Jonnalagadda, S. V.; Balsara, N. P.; Han, C. C.; Krishnamoorti, R. Macromolecules 1996, 29, 661.
39. Lefebvre, A. A.; Lee, J. H.; Balsara, N. P.; Hammouda, B.; Krishnamoorti, R.; Kumar, S. Macromolecules 1999, 32, 5460.
40. Lefebvre, A. A.; Lee, J. H.; Balsara, N. P.; Hammouda, B. J Polym Sci Part B: Polym Phys 2000, 38, 1926.
41. Lefebvre, A. A.; Lee, J. H.; Balsara, N. P.; Hammouda, B. Macromolecules 2000, 33, 7977.
42. Lefebvre, A. A.; Balsara, N. P.; Lee, J. H.; Vaidyanathan, C. Macromolecules 2002, 35, 7758.
43. Staverman, A. J.; Van Santen, J. H. Recl Trav Chim 1941, 60, 76.
44. Huggins, M. L. J Phys Chem 1942, 46, 151.
45. Flory, P. J. J Chem Phys 1942, 10, 51.
46. Computing the binodal and spinodal curves with eqs 2–4 also requires knowledge of the temperature and pressure dependence of v_i. These values were obtained from pressure–volume–temperature data for the pure components (see refs. 47 and 48).
47. Krishnamoorti, R. Ph.D. Thesis, Princeton University, 1994.
48. Lefebvre, A. A. Ph.D. Thesis, University of California at Berkeley, 2002.
49. The RPA analysis of the static scattering profiles requires knowledge of both χ parameters and statistical segment lengths. Details regarding the fitting procedure are given in ref. 41. The statistical segment lengths obtained from our fits are within the experimental error (10%) of the literature values.
50. Polymer Blends; Paul, D. R.; Newman, S., Eds.; Academic: San Diego, 1978; Vols. 1 and 2.
51. The OZ analysis was restricted to quench depths at which no peaks were observed during the early stages; see ref. 30 for details.
52. Cahn, J. W. Trans Am Inst Miner Metall Pet Eng 1968, 242, 166.
53. Calculating the phase diagram in χN-versus-ϕ format for a binary blend requires defining N and $\chi(T,P)$ on the basis of the same reference volume. To obtain the curves in Figure 10, we assume that $N = (N_1 v_1 + N_2 v_2)/2v_0$ (N_1, N_2, v_1, v_2, and v_0 are defined in eq 1).
54. Okada, M.; Han, C. C. J Chem Phys 1986, 85, 5317.
55. Bates, F. S.; Wiltzius, P. J Chem Phys 1989, 91, 3258.
56. Schwahn, D.; Janssen, S.; Springer, T. J Chem Phys 1992, 97,8775.
57. Jinnai, H.; Hasegawa, H.; Hashimoto, T.; Han, C. C. J Chem Phys 1993, 99, 4845.
58. Jinnai, H.; Hasegawa, H.; Hashimoto, T.; Han, C. C. J Chem Phys 1993, 99, 8154.